HHS Public Access

Author manuscript

Colloids Surf B Biointerfaces. Author manuscript; available in PMC 2017 March 02.

Published in final edited form as:

Colloids Surf B Biointerfaces. 2016 September 01; 145: 768–776. doi:10.1016/j.colsurfb.2016.05.086.

Topographic guidance based on microgrooved electroactive composite films for neural interface

Xiaoyao Shi[a], **Yinghong Xiao**[b,d], **Hengyang Xiao**[a], **Gary Harris**[c], **Tongxin Wang**[b,c,**], and **Jianfei Che**[a,c,*]

[a]Key Laboratory of Soft Chemistry and Functional Materials, Ministry of Education, Nanjing University of Science and Technology, Nanjing 210014, China

[b]College of Dentistry, Howard University, Washington, DC 20059, USA

[c]College of Engineering, Howard University, Washington, DC 20059, USA

[d]Collaborative Innovation Center for Biomedical Functional Materials, Nanjing Normal University, Nanjing 210046, China

Abstract

Topographical features are essential to neural interface for better neuron attachment and growth. This paper presents a facile and feasible route to fabricate an electroactive and biocompatible micro-patterned Single-walled carbon nanotube/poly(3,4-ethylenedioxythiophene) composite films (SWNT/PEDOT) for interface of neural electrodes. The uniform SWNT/PEDOT composite films with nanoscale pores and microscale grooves significantly enlarged the electrode-electrolyte interface, facilitated ion transfer within the bulk film, and more importantly, provided topology cues for the proliferation and differentiation of neural cells. Electrochemical analyses indicated that the introduction of PEDOT greatly improved the stability of the SWNT/PEDOT composite film and decreased the electrode/electrolyte interfacial impedance. Further, in vitro culture of rat pheochromocytoma (PC12) cells and MTT testing showed that the grooved SWNT/PEDOT composite film was non-toxic and favorable to guide the growth and extension of neurite. Our results demonstrated that the fabricated microscale groove patterns were not only beneficial in the development of models for nervous system biology, but also in creating therapeutic approaches for nerve injuries.

Keywords

Topographic guidance; Microgrooved structure; Conductive composite film; Neural interface

1. Introduction

The wide application of neural electrodes in modern medical therapies has revealed great benefit for patients suffering from neural impairment and disorder, such as deafness,

*Corresponding author at: Nanjing University of Science and Technology, Key Laboratory of Soft Chemistry and Functional Materials, Ministry of Education, Nanjing 210014, China. **Corresponding author at: College of Dentistry, Howard University, Washington, DC 20059, USA.

Parkinson's disease, epilepsy, blindness, intractable pain, and paralysis [1–3]. Currently, one of the major problems that affect clinical applications of neural electrodes is the inconsistent performance during the long-term implantation [4].

Nanoscale components at the neural interface are crucial factors for excellent neural devices due to the complex nanoscale structural features of neural tissue. The challenge for materials science is to apply nanotechnology strategies to fabricate biologically mimic materials which is soft, ionic, wet, and dynamic [5]. Several strategies have been proposed to improve the electrical properties and reactive tissue responses of neural electrodes, such as surface modification with bioactive conductive materials with nanostructures [6–10]. Surface modification with carbon nanotubes (CNTs) or conducting polymers (CP) such as polypyrrole (PPy) and poly(3,4-ethylenedioxythiophene) (PEDOT) can provide an excellent foundation for neural electrode design focused on improving the charge storage capacity and decreasing the interfacial impedance with neurons [11–13]. Additionally, the nanoscale structures of the CNT films and CP coatings can influence the subcellular behaviors including the organization of the cell adhesion molecule receptors, proliferation and differentiation to enhance the communication between biological and electrical systems [14].

Recent studies have shown that cellular behavior can be guided by both chemical signals and physical interactions at the cell-substrate interface [15,16]. Neurons are capable of sensing and responding to biophysical cues, over a wide range of length scales. Guiding and promoting neurite outgrowth are essential neuron growth procedures during nerve regeneration [16]. Therefore, while it is important to construct a variety of biocompatible nanoscale conductive materials at the electrode interface, it is still desired for biomedical applications to provide additional physical guidance cues for cells. When micropatterns are introduced into the bioactive conductive coatings, cellular and supracellular characteristics such as cell morphology and migration, and tissue organization will be influenced, which is necessary for neural electrodes or nerve conduits to create surfaces that can modulate neuron response to the implanted devices [17,18].

Microscale groove patterns are among the most common fabricated topographical features that have been employed to control cell behavior [19]. The majority of cell types cultured on this topography align along the major axis of grooves, with their alignment and orientation enhanced on decreased groove width and increased groove depth [20]. Fabrication of microscale grooves mostly relies on conventional photolithography, which is widely used to generate rigid microstructures on inorganic materials, such as silicon and titanium oxide [21,22]. Soft lithography also has been developed to fabricate grooves, which uses elastomeric polymers to develop patterns based on embossing, molding, and printing methods [23]. However, the bioactive conductive coatings with microscale groove patterns cannot be introduced onto the surface of metal electrodes via these techniques directly.

Some specific approaches have been found to fabricate conductive coatings with grooves on the metal electrodes, including electro-beam lithography [24] and laser-ablation [25], which generally need high energy supply. In this paper, we proposed a facile and effective approach to fabricate CNT/CP composite coatings with topographical feature: nanoscale pores and

microscale grooves. In particular, aligned microscale poly(lactic acid) (PLA) fibers obtained by electrospinning were used as template for electrophoretic deposition of the single-walled carbon nanotube (SWNT) films. After removing the PLA fibers by dissolving the films in dichloromethane, hollow tubes were formed in the SWNT films. The hollow tubes were broken easily in an ultrasonic bath to obtain grooved structures. PEDOT was subsequently deposited onto the SWNT films by pulse electro-polymerization. The approach allows PEDOT to form an ultrathin coaxial layer around the SWNT bundles throughout the whole film to remain the micro- and nanoscale structures of the SWNT films. PEDOT was employed in this study as the conducting polymer coating due to its highly ordered chemical structure and thus stable electrochemical properties [26,27]. Compared with thiophene, when an ethylenedioxy bridge is fused onto the 3- and 4-positions of the thiophene ring, the resulting 3,4-ethylenedioxythiophene (EDOT) monomer possesses a lower band-gap and polymer oxidation potentials. Electrochemical analyses indicated that the introduction of PEDOT greatly improved the stability of the SWNT/PEDOT composite film and decreased the electrode/electrolyte interfacial impedance. Further, in vitro culture of rat pheochromocytoma (PC12) cells showed that the grooved SWNT/PEDOT composite film was non-toxic and favorable to guide the growth and extension of neurite.

2. Materials and methods

2.1. Materials

SWNTs synthesized by electric arc discharge were purchased from Carbon Solutions Inc. (CSI, Riverside, CA). The nanotubes have an average diameter of 1.4 nm and individual tube lengths ranging from 0.5 to 3 μm. EDOT (97%) and dimethyl-sulfoxide (DMSO) was purchased from Sigma-Aldrich (St. Louis, MO). 3-(4,5-Dimethylthiazol-2-yl)-2,5-diphenyltetrazolium bromide (MTT) was obtained from Amresco (Bioscience, Shanghai, China). The reagents used in cell culture including Dulbecco's modified Eagle's medium (DMEM), fetal bovine serum, horse serum, L-glutamine, streptomycin, and penicillin, were purchased from Nanjing Tengchun Bio-technology Development Co., Ltd (Nanjing, China). PLA (4032D) was purchased from NatureWorks (Blair, NE).

All other reagents of analytical grade were obtained from Shanghai Chem. Co. (Shanghai, China) and used as received without further purification.

2.2. Modification of the electrode surface

2.2.1. Fabrication of the aligned PLA fiber template—Stainless metal was cut into small square electrodes with size of 2.0 × 0.5 cm^2. Before use, the electrodes were bathed in 1 M NaOH at 100 °C for 1 h and washed subsequently with acetone, deionized (DI) water and ethanol. The aligned PLA fibers were obtained by electrospinning on static parallel electrodes [28]. In detail, 0.36 g PLA was dissolved in 3.25 g chloroform/ethanol solution (75/25, v/v) at room temperature and stirred for 5 h to obtain a homogenous solution with PLA concentration of 10 wt%. PLA was directly electrospun onto the gap between the static parallel electrodes in an electrical field of 0.7 kV cm^{-1} with a flow rate of 0.25 mL h^{-1} for min. The static parallel electrodes with a gap of 1 cm were held at a distance of 10 cm from

the syringe needle. Finally, the aligned PLA fibers were transferred onto stainless metal electrodes for further use.

2.2.2. Electrophoretic deposition of the SWNT film—SWNT film was deposited by electrophoretic deposition onto the above PLA fiber-covered electrodes. Before deposition, SWNTs were purified and carboxylated under water bath sonication in a sulfuric-nitric acid (3:1, v/v) at 60 °C for 4h. The mixture was diluted with water, filtered through a 0.22 μm filter and washed thoroughly with DI water until the pH value reached *ca* 6.0. The functionalized SWNTs were then recovered from the filter and redispersed in ethanol under ultrasonication, resulting in a stable and homogeneous solution with SWNT concentration of 0.5 mg mL^{-1}. 75 μL of 0.1 M $Al(NO_3)_3$-$9H_2O$ ethanol solution was diluted to different concentrations, followed by the addition of 0.5 mL SWNT dispersion for electrophoresis. The PLA-covered electrodes were immersed in the dispersion in an electrophoresis cell, with an electrode gap of 1 cm. Care was taken to ensure that the electrodes were parallel to each other. Direct current (DC) voltage of 50 V was applied to deposit a SWNT film on the cathode for 5 min. The nominal area of the SWNT film was 5 × 10 mm^2. After deposition, the electrodes were dried in a desiccator at room temperature for 30 min before soaking in 0.6 M H_3PO_4 for 15 min to remove any $Al(OH)_3$ which may influence the conductivity of the SWNT film. Then the electrodes were washed with DI water and ethanol to remove any ions adsorbed on the surfaces of the SWNTs. After drying in air for 30 min, the electrodes were soaked in dichloromethane for 5 min to dissolve the PLA fibers. Finally, the electrodes were immersed in the ethanol and placed in an ultrasonic bath and removed after 5 s before another immersion. The repetitive immersion was performed to apply the effect of ultrasonic vibration intermittently, inhibiting the rapid progression of the groove formation.

2.2.3. Fabrication of the grooved SWNT/PEDOT composite film—Pulse electro-polymerization was performed in an aqueous solution of 0.01 M EDOT with 0.1 M *p*-toluenesulfonic acid sodium (TsONa) as dopant to produce PEDOT. The electrochemical deposition was carried out in a three-electrode system (Autolab PGSTAT302N, Ecochemie, Netherlands), using the grooved SWNT-coated stainless metal as working electrode (working area of 5 × 10 mm^2), a platinum wire as counter electrode and a standard Ag/AgCl electrode as reference electrode. The working potential was programmed with a waveform consisting of a potential step to 1.0 V for the deposition time (T_d) of 5 s followed by switching off for a rest time (T_r) of 600 s. This waveform was repeated for 8 cycles for a total polymerization time of 40 s. After polymerization, the SWNT/PEDOT composite film was washed repeatedly with DI water to remove any remaining electrolyte and monomer and dried in air.

2.3. Characterization

Surface morphologies of the films were observed by field emission scanning electron microscopy (FESEM, JSM-7600F, JEOL Ltd., Japan) and optical microscopy (OM, NMR-800RF/TRF, Novel optical, China). The alignments were quantified by an ImageJ image processing software. To tell the elemental distribution in the grooved structures, energy dispersive spectroscopy (EDS) was recorded using FESEM. Infrared spectra (FTIR) of SWNT, PEDOT and SWNT/PEDOT were recorded with a Shimadzu FTIR-84 using KBr

pellets. Raman spectra were collected across the 400–4000 cm^{-1} region (Renishaw, RM2000, Britain), using the 578.5 nm line of an Ar^{+} laser as its excitation source. Cyclic voltammograms (CV) was performed in 0.1 M KCl aqueous solution containing 1 mM $[Fe(CN)_6]^{3-/4-}$ (1:1) in a potential range of −0.4–0.7 V (vs. saturated calomel electrode) at a scan rate of 50 mV s^{-1}, using the General Purpose Electrochemical Systems data processing software (GPES, software version 4.9). Electrochemical impedance spectroscopy (EIS) was carried out in 0.1 M phosphate buffered saline (PBS, pH = 7.4) in a range from 0.01 to 100 kHz with an amplitude of 10 mV. All solutions were deaerated by bubbling nitrogen prior to experiments and the electrochemical cell was kept in a nitrogen atmosphere throughout the experiments. Zview software (Scriber Associates, Inc., USA) were employed for the curve fitting analyses. UV spectra were recorded using a UV-vis spectrophotometer (model Lambda Bio 20, Perkin-Elmer Co., USA).

2.4. Cells culture

PC12 cells were maintained in a tissue culture dish or flask in a growth medium composed of DMEM, supplemented with heat-inactivated fetal bovine serum (10% volume), heat-inactivated horse serum (5%), L-glutamine (2 mm), streptomycin (100 mg mL^{-1}) and penicillin (100 units mL^{-1}), and were incubated in CO_2 (5%) and O_2 (95%). The medium was changed every 2–3 days. The electrodes were sterilized using UV irradiation for about 1 h at room temperature immediately before cell culture. The cells were cultured for about 7 days to ensure that all cells adhered tightly to the substrate surface and multiplied to the desired density. After cell culture, the cell morphologies were monitored using an Axiovert 200 Motorized Inverted Microscope System (Carl Zeiss Vision GmbH) and pictured with a digital CCD camera using Axio-vision 4.0 software. For FESEM observation, the samples were first rinsed with PBS to remove medium components and non-adhered cells and fixed with glutaraldehyde (2.5%) in PBS for 1 h. Then the samples were immersed into 30% and 50% ethanol in PBS and sequentially dipped in three ethanol/water solutions (70/30, 90/10 and 100/0, v/v), respectively for 15 min. Finally, the samples were socked in hexamethyldisilazane (HMDS) for 15 min to completely remove H_2O from the cells.

To further assess the cytotoxicity of the coated electrodes and quantify the cell growth, in vitro MTT assay was applied. MTT was dissolved in PBS (pH 7.4) to a concentration of 5.0 mg mL^{-1} and stored at −20 °C. PC12 cells were cultured on the electrodes with different surfaces, with a seeding density of 2×10^5 cells cm^{-1}. The electrodes were placed in 24-well plates with 200 μL complete culture media in each well before the plates were placed in an incubator at 37 °C with 5% CO_2. After 6 d of incubation, the media were removed and subsequently replaced with MTT solution, followed by incubation for another 5 h. After incubation, the media was removed followed by adding 200 μL DMSO to each well to dissolve the produced formazan crystal. The mixture was shaken for 10 min before UV absorbance measurements at 490 nm were performed.

Cell survival percentage was calculated according to the following equation:

$$\text{Survival percentage } (\%) = \frac{A_s}{A_c} \times 100\%$$

where A_S is the absorbance of the sample and A_c the absorbance of the blank control.

A Student *t*-test was used to assess the significance between means of two groups. $p < 0.05$ was considered statistically significant.

3. Results and discussion

3.1. Microscale groove patterns

FESEM was employed to validate the formation of the grooved SWNT films deposited on the electrodes. As seen in Fig. 1a, the diameter of the PLA fibers varies from 1 to 2 μm. The alignment of the fibers was quantified by using OM and an ImageJ image processing software. Fibers for OM were deposited on glass slides and the images were collected under brightfield conditions. The angles (*h*) between the long axes of the fibers and their expected direction (parallel to the vectors of the magnetic field) were employed as a parameter to quantify the alignment. From the corresponding statistical analysis on alignment, a conclusion can be drawn that most fibers aligned in the desired direction, i.e. perpendicular to the magnets (more than 90% of the fibers are within 15° scope of this direction). PLA fibers with good alignment were obtained via electrospinning and transferred onto the stainless metal electrodes. After electrophoretic deposition, the whole electrode surface was covered with a uniform SWNT thin layer, as displayed in Fig. 1b. The thickness of the SWNT film can be controlled through adjusting the parameters of electrophoretic deposition, including deposition voltage, deposition time and concentration of SWNT dispersion. PLA was considered as suitable polymers for the template since they can be readily processed into nanoscale fibers, are stable during electrophoretic deposition, and can be easily removed under conditions to leave the wall material intact [29]. After soaking in dichloromethane for 5 min, the PLA nanofibers can be removed completely, which can be confirmed by the tunnel structure of SWNT in SEM image. To better observe the structure, we controlled the sonication intensity to obtain SWNT tunnels on the electrodes. As shown in Fig. 1c, the SWNT tunnels are hollow tubes as expected after the dissolution experiment. The inset in Fig. 1c shows the hollow structure of SWNT with well-defined internal and external texture. The internal texture is replicated from the external texture of PLA electrospun nanoscale fibers. The hollow structures are weak and can be easily destroyed by ultrasonication. As shown in Fig. 1d, the grooved structures were thus obtained through the repetitive immersion of the electrode shown in Fig. 1b in an ultrasonic bath. The diameter of the grooves is almost two times of the fiber diameter. It is worthy to note that the thickness of the SWNT film needs to be well adjusted to make sure that the hollow structures can be completely destroyed to achieve a uniform grooved surface topography.

Fig. 2. shows the FESEM images of the grooved SWNT/PEDOT composite films obtained through the pulse electropolymerization. In a constant potential mode, the deposition mainly occurs on the SWNT external surface rather than on SWNT bundle surfaces in the inner space [30]. This is due to the fact that the monomers do not have sufficient time to diffuse into the SWNT films, which may result in a blockage of the pores in the SWNT films. In cellular structure materials, the deposition rate of conducting polymer is controlled by the balance of two factors, the polymerization rate and the diffusion rate of monomers into the interior of the material. Generally, the former is far faster than the latter so that the diffusion

rate of the monomers is the determinant factor to the final deposition rate of the conducting polymer on the electrode. With the pulse electro-polymerization mode, the long “off” intervals allow EDOT monomers in the supporting electrolyte to diffuse into the space between SWNT bundles throughout the entire films and the brief “on” pulses confine polymer deposition and growth on the SWNT surfaces, leading to the formation of uniform and coaxial layers of PEDOT on the surfaces of the SWNT bundles [31]. With this strategy, the microscale groove patterns can be well retained due to the fact that the polymerization on the SWNT film external surfaces is avoided. The patterns are combined with the nanoscale pores to form a special topography, which is favorable for controlling cell adhesion, promoting cell alignment, and improving biocompatibility.

EDS mapping was applied to demonstrate the grooved structure by the distribution of different elements (Fig. 3). It is obviously seen that less C is distributed in the area of the groove due to the absence of the SWNTs. The distribution ununiformity of O in the groove is not that obvious but still can be identified. This can be explained by the fact that C comes mainly from the SWNTs thus the signal for C in the grooved area is greatly weakened. However, the signal for O is complemented by the relatively higher O content in PEDOT molecules, compared to the O content in SWNTs. The results again confirm the microscale groove patterns fabricated with our strategy. S only comes from PEDOT thus is distributed uniformly in the entire composite film.

3.2. Chemical structure of the SWNT/PEDOT composite film

FTIR was performed to confirm the presence of PEDOT in the SWNT film (Fig. 4 A). For the SWNTs, the peaks at 1125 cm^{-1} is assigned to the stretching vibration of C-C-O, 1386 cm^{-1} to the graphite wall, 1629 cm^{-1} to the stretching vibration of C O and 3422 cm^{-1} to the −OH and −COOH functional groups introduced by the acid treatment [32]. The FTIR spectrum of PEDOT exhibits the main characteristic bands as follows. The band around 630 cm^{-1} is due to the deformation vibration of the thiophene ring [33]. Vibrations at 1509 and 1386 cm^{-1} are attributed to the stretching modes of C=C and C–C in the thiophene ring [34]. The peaks at 1086 cm^{-1} and 1125 cm^{-1} are attributed to deformation vibration and stretching vibration of C–O–C, respectively [35]. The band around 840 cm^{-1} is due to the ethylenedioxy ring deformation mode. The vibration modes from the C-S bond in the thiophene ring can be seen at 974 cm^{-1} [36]. In the spectrum of the SWNT/PEDOT composite films, no extra peaks are observed except for the characteristic peaks of the two components. This suggests that no new chemical bonds are formed between the SWNTs and PEDOT in the SWNT/PEDOT composite films.

To better understand the interaction between the SWNTs and PEDOT, Raman characterization was performed (Fig. 4B). It is known that SWNTs represent the typical peaks located at *ca.* 1332 and 1582 cm^{-1}, corresponding to the D band and G band, respectively. As for PEDOT, the peak at 1436 cm^{-1} is attributed to the symmetric C=C stretching vibration while the peak at 1510 cm^{-1} is assigned to the antisymmetric C=C stretching vibration. The characteristic Raman bands for SWNTs and PEDOT are present in the spectrum of the SWNT/PEDOT composite. However, we notice that with interacting with the nanotubes the shifts of C=C stretching vibration of PEDOT move to low

wavenumbers (1425 and 1502 cm^{-1} for symmetric and antisymmetric C=C stretching vibration, respectively). The C=C stretching vibrations reflect the electronic structure thus the shift in the band positions can tell the change of the electron distribution. This phenomenon implies a fact that there is a strong conjugation interaction between the SWNT rings and PEDOT rings in the composite, which may decrease the electron density of PEDOT and cause a red shift of C=C vibrations.

3.3. Electrochemical performance

3.3.1. Cyclic voltammograms—The electrochemical properties of the modified electrodes were studied by CV, which is normally used to evaluate the redox characteristics and the charge storage capacity of the electrodes. In order to better understand the electrochemical features and stability, the electrodes were scanned between −0.4 and 0.7 V (vs. Ag/AgCl) to avoid the insulation at very negative potentials and over-oxidization at positive potentials of the polymer films. As can be seen in Fig. 5A, the cathodic charge storage capacity (*CSCc*) of the electrodes is increased from 1.90 to 3.65 and 3.92 mC cm^{-2} after the electrophoretic deposition of SWNTs and the pulse electropolymerization of PEDOT, respectively. It implies that the deposited CNTs and PEDOT can significantly improve the capacitive property of the metal electrodes. As can be observed in Fig. 5A, the peak current in CV for the grooved SWNT/PEDOT is much higher than that of the bare electrode under the same conditions, implying that the deposition of SWNT/PEDOT results in a coating with a higher specific surface area. The SWNT/PEDOT coated electrode with largely increased surface area possesses more electroactive sites for the electrodes to carry out redox reactions, leading to increased peak currents.

As a potential candidate for the electrode material applied to neural electrodes, the stability of the composite film is a crucial performance for its long-term use. Hence, it is necessary to investigate the stability of the grooved SWNT/PEDOT film. It is known that modification of the shape of the voltammogram upon potential cycling can be related to many factors, such as degradation of the polymer. Fig. 5B shows the changes of redox behavior of different electrodes scanned for 200 cycles. The changes of *CSCc* were used to evaluate the stability of the coating, because the *CSCc* reflects the electroactivity of the electrode. The *CSCc* loss of the grooved SWNT and grooved SWNT/PEDOT electrodes was 26.1% and 13.2%, respectively, indicating that the SWNT/PEDOT coated electrode exhibits good electrical stability compared with the SWNT coated electrode. For SWNTs, the integration of the film was built through van der Waals forces. Some SWNTs may separate from the whole film and migrate into the electrolyte solution during the cyclic sweeping. After the following electrochemical polymerization, PEDOT would bind SWNT surfaces in a helical structure due to the chirality interchain attractions between the polymer and CNTs [37]. The helical growth rule guides the EDOT monomers to assemble onto the PEDOT molecular chain, making the PEDOT chains wrap the SWNT bundles and effectively inhibits the migration of SWNTs. The CV variation of the 1st and 200th cycles for the SWNT coated electrode with PLA template was shown in Fig. 5B as control. There is no noticeable difference between the surface characteristics prior and after the removal of the PLA fiber template in the first cycle. However, it is clearly seen that after 200 cyclic sweeping, the redox property of the electrode with PLA template was further decreased compared to that of grooved SWNT.

This can be explained by the fact that in the sweeping process part of the SWNTs were exfoliated from the convex PLA fibers, making the organic fibers exposed to the electrolyte.

To understand the redox kinetics of the modified electrode, CV measurements of the grooved SWNT/PEDOT film at various scan rates were performed. From the plots shown in Fig. 5C, it is noticed that with increasing scan rate from 25 to 200 mV s^{-1}, the separation of redox potential ΔE_p changes from 137 to 411 mV, indicating a quasi-reversible electrochemical kinetics. Meanwhile, both anodic and cathodic peak currents increase with increasing scan rate. The inset in Fig. 5C displays the relationship between the peak current (I_{pa} and I_{pc}) and the square root of scan rate $v^{1/2}$ ($I_{pc} = 0.07998\ v^{1/2} - 0.21569$, $I_{pa} = -0.08208\ v^{1/2} + 0.24746$). The linear relationship indicates that the electrochemical reaction at the electrode-electrolyte interface is a diffusion-controlled process.

3.3.2. Electrochemical impedance spectroscopy—Neural electrodes facilitate the functional stimulation and recording of impulses from the neurons in peripheral and central nervous systems. Low impedance in the neural interface is important when an electrode serves in the transmission of stimulation pulses of neural signals. EIS is an attractive method to study the electrical behavior of coated and uncoated neural prosthetic devices. It involves measuring the electrode impedance over a spectrum of frequencies. Not only can it determine the magnitude of the resistive and capacitive response, but it can also examine their performance over a wide range of frequencies. By using these data, one can obtain qualitative and quantitative information about the electrical properties of the modified electrodes. One kilohertz is the frequency characteristic of neural biologic activity; therefore, impedance at this point is frequently used as a standard to evaluate a neural electrode [38]. In our study, the impedance was measured over a range of frequencies from 10^{-2} to 10^5 Hz. The electrochemical properties of the grooved SWNT and grooved SWNT/PEDOT films are shown in Fig. 5D. The impedance modulus of bare metal electrode is sharply decreased within the whole frequency range after coating with the grooved SWNT, particularly in the lower frequency region. In addition, the deposition of PEDOT progressively decreases the impedance of the coated electrode. At 10^3 Hz, the impedance decreases from 29.3 Ω of metal electrode to 9.8 Ω of grooved SWNT/PEDOT electrode. This can be possibly explained by the increase of an effective surface area (as shown in SEM) and the enhanced intra-bundle connections between the tubes.

3.4. Cell culture

Biocompatibility is an important property for the materials applied to the surface modification of metal electrodes. To determine the biocompatibility of the different coatings, the modified electrodes were used as substrates for neural cell culture as well as MTT testing was employed to compare the cytotoxicity of the bare electrode, SWNT, SWNT/PEDOT and grooved SWNT/PEDOT. As a neural model cell line, PC12 cells were used to investigate neuronal adhesion, neurite outgrowth and cell viability. Fig. 6 shows the images of PC12 cells grown on different substrates for 7 days. Compared to the cultures on the bare substrate where the neurons are not well attached (Fig. 6a), it is clear that the neurons grow evenly over the entire coatings and show observable difference (Fig. 6b–d). The phenomena demonstrate that the surface roughness plays a significance role in cell attachment. Since

SWNTs were encapsulated with PEDOT, there is less possibility for the tubes to diffuse into the surrounding environment and directly exposed to the soft cells. As a result, the biocompatibility of the composite film is dramatically improved, thus robust neuronal growth on the SWNT/PEDOT substrates can be observed (Fig. 6c–d) in comparison with that on the pure SWNT coating (Fig. 6b). Moreover, neurons cultured on the grooved SWNT/PEDOT coatings display observable directional growth (Fig. 6d). Further characterization was carried out with SEM to show detailed morphology of the cell growth. As can be seen in Fig. 6e and f, the neurons are tightly attached to the SWNT/PEDOT composite surface and present positive neurite extensions. Particularly, the PC12 cells cultured on the grooved SWNT/PEDOT coatings were ovally shaped overlying the substrate, and the neurite differentiated along the direction of the grooves. The responses to topography are thought to be transduced by tension generated within the cytoskeleton and the redistribution of focal adhesion complexes (FAC) thanks to the preferred patterns [39]. Additionally, the cytoskeleton is directly connected to the nuclear membrane that ultimately alters nuclear morphology, which has been hypothesized to be connected to changes in gene expression [39,40]. We concluded that the grooved SWNT/PEDOT composite film has a potential application in neural electrodes and nerve conduits where the orientation of neurons is necessary.

In MTT testing, the cell survival was directly proportional to the amount of the formazan produced, which was monitored by the UV absorbance at 490 nm. Cell viability on different electrode substrates is shown in Fig. 7. PC 12 cells do not show preference on bare metal electrode or SWNTs due to their incompatible surface features, revealed by the low survival percentage of 40% and 60% respectively. On the contrary, the viability of cells cultured on SWNT/PEDOT surface is much higher, demonstrating that SWNT/PEDOT is a promising nanocomposite for the surface modification of neural prosthetic devices. More important, the cells are favorable to grow on the grooved SWNT/PEDOT. The cell viability has no noticeable difference from that of the cells cultured in complete media. The results are in good agreement with those shown in Fig. 6a–f, indicating the excellent biocompatibility and low cytotoxicity of the SWNT/PEDOT coating and the priority of the grooved SWNT/PEDOT.

4. Conclusions

Our study provides a simple and feasible way to fabricate micropatterned SWNT/PEDOT composite films on metal electrodes. The uniform SWNT/PEDOT composite films with nanoscale pores and microscale grooves can significantly enlarge the electrodeelectrolyte interface, facilitate ion transfer within the bulk film, and provide topology cues for the proliferation and differentiation of neural cells. In particular, the R_{ct} dramatically decreased from 1.063×10^7 Ω for bare electrodes to 6.469×10^4 Ω for grooved SWNT/PEDOT coated electrodes. The enhanced intra-bundle connections and the strengthened network connection of SWNT bundles through deposition of PEDOT greatly improved the stability of whole composite films. The *CSCc* loss after 200 cycles CV tests decreased 26.1% for grooved SWNT coated electrode and 13.2% for grooved SWNT/PEDOT coated electrodes respectively, indicating the better electric stability of the latter, which is crucial for long-term implantation applications. Moreover, the grooved SWNT/PEDOT composite films exhibit

excellent biocompatibility compared to the randomly packed SWNT films and is able to provide additional physical guidance cues for neurite extensions.

Acknowledgments

The project was supported by the Specialized Research Fund for the Doctoral Program of Higher Education of China (20123219110010) and Priority Academic Program Development of Jiangsu Higher Education Institutions of China (PAPD), partially by NSF Grant of the USA (DMR1231319), NIH/NIDCR Grant of the USA (R01 DE021786), and US ARMY Grant (W911NF-15-1-0051).

References

1. Cogan SF. Neural stimulation and recording electrodes. Annu. Rev. Biomed. Eng. 2008; 10:275–309. [PubMed: 18429704]
2. Macherey O, Carlyon RP. Cochlear implants. Curr. Biol. 2014; 24:R878–R884. [PubMed: 25247367]
3. Thompson DM, Koppes AN, Hardy JG, Schmidt CE. Electrical stimuli in the central nervous system microenvironment. Annu. Rev. Biomed. Eng. 2014; 16:397–430. [PubMed: 25014787]
4. Grill WM, Norman SE, Bellamkonda RV. Implanted neural interfaces: biochallenges and engineered solutions. Annu. Rev. Biomed. Eng. 2009; 11:1–24. [PubMed: 19400710]
5. Wallace GG, Spinks GM. Conducting polymers: a bridge across the bionic interface. Chem. Eng. Prog. 2007; 103:S18–S24.
6. Chen S, Pei W, Gui Q, Tang R, Chen Y, Zhao S, Wang H, Chen H. PEDOT/MWCNT composite film coated microelectrode arrays for neural interface improvement. Sensor Actuat. A: Phys. 2013; 193:141–148.
7. Mandal HS, Knaack GL, Charkhkar H, McHail DG, Kastee JS, Dumas TC, Peixoto N, Rubinson JF, Pancrazio JJ. Improving the performance of poly (3,4-ethylenedioxythiophene) for brain–machine interface applications. Acta Biomater. 2014; 10:2446–2454. [PubMed: 24576579]
8. Siriwardane ML, DeRosa K, Collins G, Pfister BJ. Controlled formation of cross-linked collagen fibers for neural tissue engineering applications. Biofabrication. 2014; 6:015012. [PubMed: 24589999]
9. Charkhkar H, Knaack GL, McHail DG, Mandal HS, Peixoto N, Rubinson JF, Dumas TC, Pancrazio JJ. Chronic intracortical neural recordings using microelectrode arrays coated with PEDOT–TFB. Acta Biomater. 2016; 32:57–67. [PubMed: 26689462]
10. Gutowski SM, Shoemaker JT, Templeman KL, Wei Y, Latour RA, Bellamkonda RV, LaPlaca MC, García AJ. Protease-degradable PEG-maleimide coating with on-demand release of IL-1Ra to improve tissue response to neural electrodes. Biomaterials. 2015; 44:55–70. [PubMed: 25617126]
11. Xiao H, Zhang M, Xiao Y, Che J. A feasible way for the fabrication of single walled carbon polypyrrole composite film with controlled pore size for neural interface. Colloids Surf. B. 2015; 126:138–145.
12. Fuchsberger K, Goff AL, Gambazzi L, Toma FM, Goldoni A, Giugliano M, Stelzle M, Prato M. Multiwalled carbon-nanotube-functionalized microelectrode arrays fabricated by microcontact printing: platform for studying chemical and electrical neuronal signaling. Small. 2011; 7:524–530. [PubMed: 21246714]
13. Castagnola V, Descamps E, Lecestre A, Dahan L, Remaud J, Nowak L, Bergaud C. Parylene-based flexible neural probes with PEDOT coated surface for brain stimulation and recording. Biosens. Bioelectron. 2015; 67:450–457. [PubMed: 25256782]
14. Lee JY, Schmidt CE. Amine-functionalized polypyrrole: inherently cell adhesive conducting polymer. J. Biomed. Mater. Res. A. 2015; 103:2126–2132. [PubMed: 25294089]
15. Recknor JB, Sakaguchi DS, Mallapragada SK. Directed growth and selective differentiation of neural progenitor cells on micropatterned polymer substrates. Biomaterials. 2006; 27:4098–4108. [PubMed: 16616776]
16. Song M, Uhrich KE. Optimal micropattern dimensions enhance neurite outgrowth rates, lengths, and orientations. Ann. Biomed. Eng. 2007; 35:1812–1820. [PubMed: 17616821]

17. Nikkhah M, Edalat F, Manoucheri S, Khademhosseini A. Engineering microscale topographies to control the cell–substrate interface. Biomaterials. 2012; 33:5230–5246. [PubMed: 22521491]
18. Aufan MR, Sumi Y, Kim S, Lee JY. Facile synthesis of conductive polypyrrole wrinkle topographies on polydimethylsiloxane via a swelling–deswelling process and their potential uses in tissue engineering. ACS Appl. Mater. Interfaces. 2015; 7:23454–23463. [PubMed: 26444932]
19. Kitagawa Y, Naganuma Y, Yajima Y, Yamada M, Seki M. Patterned hydrogel microfibers prepared using multilayered microfluidic devices for guiding network formation of neural cells. Biofabrication. 2014; 6:035011. [PubMed: 24876343]
20. Wang P-Y, Wu T-H, Tsai W-B, Kuo W-H, Wang M-J. Grooved PLGA films incorporated with RGD/YIGSR peptides for potential application on skeletal muscle tissue engineering. Colloids Surf. B. 2013; 110:88–95.
21. Su WT, Liao YF, Wu TW, Wang BJ, Shih YY. Microgrooved patterns enhanced PC12 cell growth, orientation, neurite elongation, and neuritogenesis. J. Biomed. Mater. Res. A. 2013; 101:185–194. [PubMed: 22829561]
22. Pérez DG, Quijorna EP, Sanz R, Torres-Costa V, Ruiz JPG, Silván MM. Nanotopography enhanced mobility determines mesenchymal stem cell distribution on micropatterned semiconductors bearing nanorough areas. Colloids Surf. B. 2015; 126:146–153.
23. Al-Haque S, Miklas JW, Feric N, Chiu LL, Chen WLK, Simmons CA, Radisic M. Hydrogel substrate stiffness and topography interact to induce contact guidance in cardiac fibroblasts. Macromol. Biosci. 2012; 12:1342–1353. [PubMed: 22927323]
24. Gomez N, Lee JY, Nickels JD, Schmidt CE. Micropatterned polypyrrole: a combination of electrical and topographical characteristics for the stimulation of cells. Adv. Funct. Mater. 2007; 17:1645–1653. [PubMed: 19655035]
25. Lasagni AF, Hendricks JL, Shaw CM, Yuan D, Martin DC, Das S. Direct laser interference patterning of poly(3,4-ethylene dioxythiophene)-poly (styrene sulfonate)(PEDOT-PSS) thin films. Appl. Surf. Sci. 2009; 255:9186–9192.
26. Luo S-C, Mohamed Ali E, Tansil NC, Yu H-h, Gao S, Kantchev EA, Ying JY. Poly(3,4-ethylenedioxythiophene)(PEDOT) nanobiointerfaces: thin, ultrasmooth, and functionalized PEDOT films with in vitro and in vivo biocompatibility. Langmuir. 2008; 24:8071–8077. [PubMed: 18588322]
27. Richardson-Burns SM, Hendricks JL, Foster B, Povlich LK, Kim D-H, Martin DC. Polymerization of the conducting polymer poly(3,4-ethylenedioxythiophene)(PEDOT) around living neural cells. Biomaterials. 2007; 28:1539–1552. [PubMed: 17169420]
28. Wong S-C, Baji A, Leng S. Effect of fiber diameter on tensile properties of electrospun poly (ε-caprolactone). Polymer. 2008; 49:4713–4722.
29. Abidian MR, Ludwig KA, Marzullo TC, Martin DC, Kipke DR. Interfacing conducting polymer nanotubes with the central nervous system: chronic neural recording using poly (3,4-ethylenedioxythiophene) nanotubes. Adv. Mater. 2009; 21:3764–3770. [PubMed: 26345408]
30. Zhang J, Kong L-B, Cai J-J, Li H, Luo Y-C, Kang L. Hierarchically porous nickel hydroxide/mesoporous carbon composite materials for electrochemical capacitors. Microporous Mesoporous Mater. 2010; 132:154–162.
31. Che J, Chen P, Chan-Park MB. High-strength carbon nanotube buckypaper composites as applied to free-standing electrodes for supercapacitors. J. Mater. Chem. A. 2013; 1:4057–4066.
32. Lee Y-K, Lee K-J, Kim D-S, Lee D-J, Kim J-Y. Polypyrrole-carbon nanotube composite films synthesized through gas-phase polymerization. Synth. Met. 2010; 160:814–818.
33. Louarn G, Mevellec J, Buisson J, Lefrant S. Experimental and theoretical-study of vibrational properties of polythiophene, polymethylthiophene and polyoctylthiophene. J. Chim. Phys. PCB. 1992; 89:987–995.
34. Garreau S, Louarn G, Buisson J, Froyer G, Lefrant S. In situ spectroelectrochemical Raman studies of poly(3,4-ethylenedioxythiophene)(PEDT). Macromolecules. 1999; 32:6807–6812.
35. Kvarnström C, Neugebauer H, Blomquist S, Ahonen H, Kankare J, Ivaska A. In situ spectroelectrochemical characterization of poly(3,4-ethylenedioxythiophene). Electrochim. Acta. 1999; 44:2739–2750.

36. Li C, Imae T. Electrochemical and optical properties of the poly(3,4-ethylenedioxythiophene) film electropolymerized in an aqueous sodium dodecyl sulfate and lithium tetrafluoroborate medium. Macromolecules. 2004; 37:2411–2416.
37. Caddeo C, Melis C, Colombo L, Mattoni A. Understanding the helical wrapping of poly(3-hexylthiophene) on carbon nanotubes. J. Phys. Chem. C. 2010; 114:21109–21113.
38. Abidian MR, Martin DC. Experimental and theoretical characterization of implantable neural microelectrodes modified with conducting polymer nanotubes. Biomaterials. 2008; 29:1273–1283. [PubMed: 18093644]
39. Dalby MJ. Topographically induced direct cell mechanotransduction. Med. Eng. Phys. 2005; 27:730–742. [PubMed: 15921949]
40. Dalby MJ, Riehle MO, Yarwood SJ, Wilkinson CD, Curtis AS. Nucleus alignment and cell signaling in fibroblasts: response to a micro-grooved topography. Exp. Cell Res. 2003; 284:272–280.

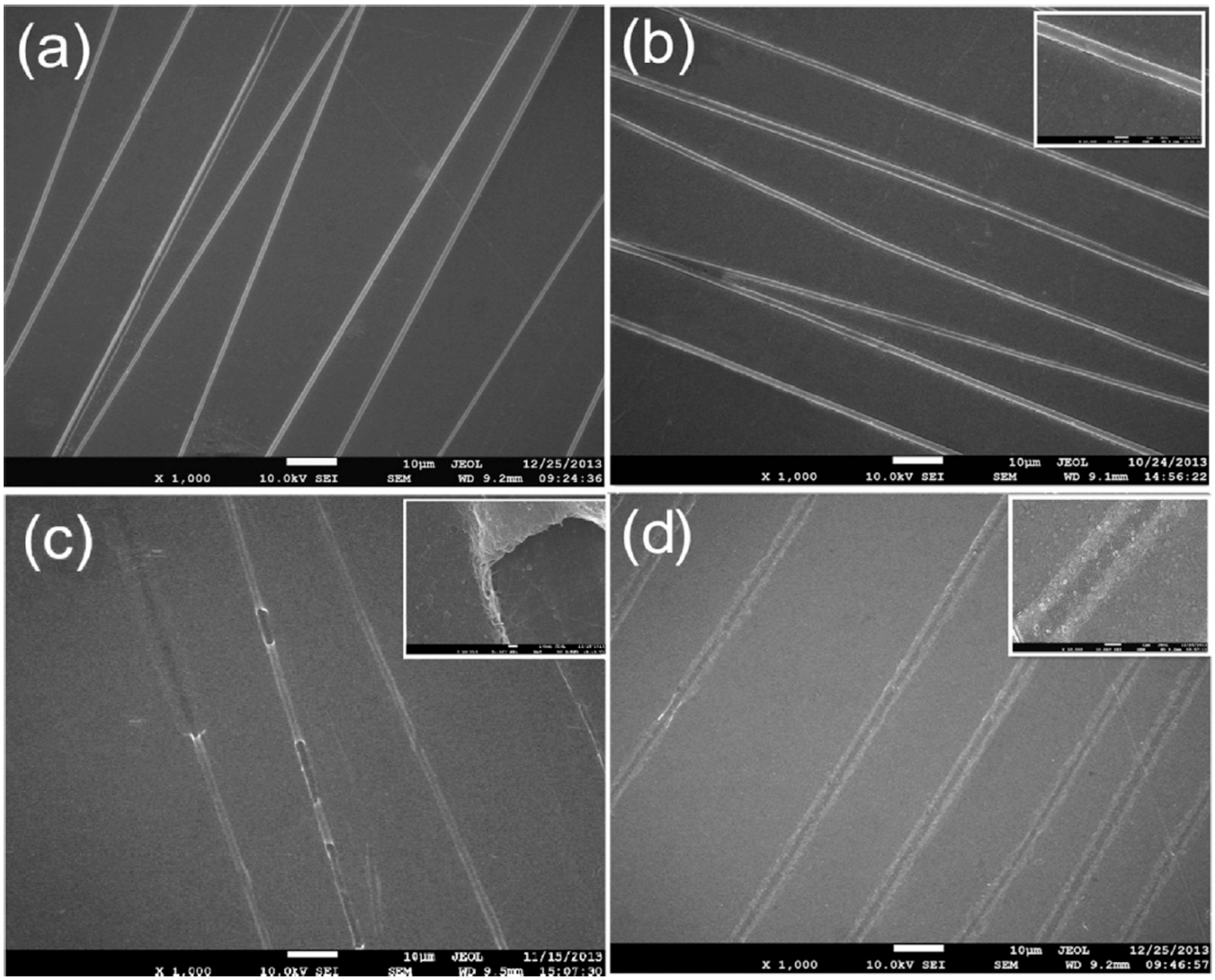

Fig. 1.

Microgrooved SWNT films fabrication: (a) Electrospinning of PLA template fibers. (b) Electrophoretic deposition of SWNT. (c) Dissolving the electrospun core fibers to create SWNT tunnels. (d) Grooved SWNT films after sonication.

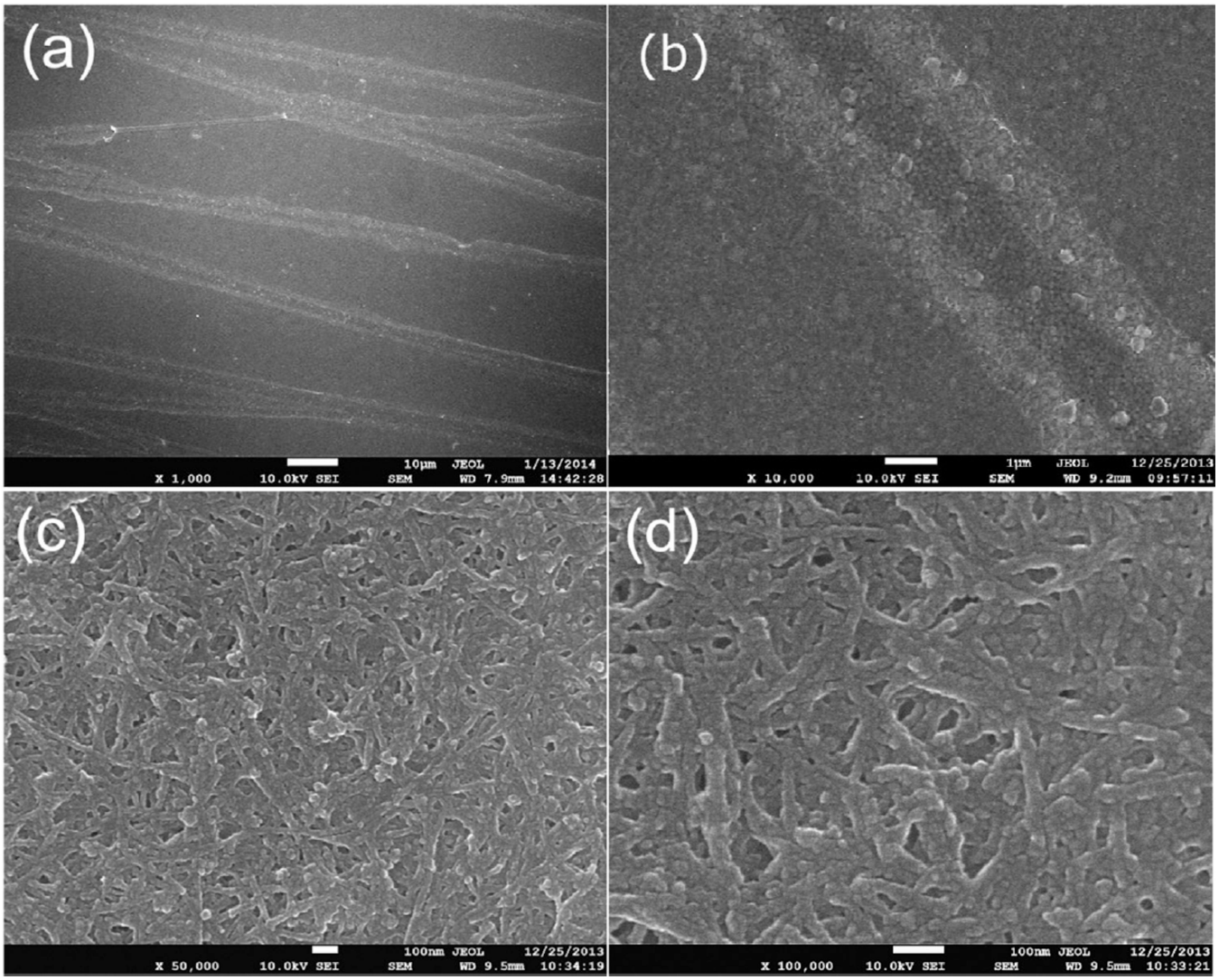

Fig. 2.
FESEM images with different magnification of the grooved SWNT/PEDOT composite films.

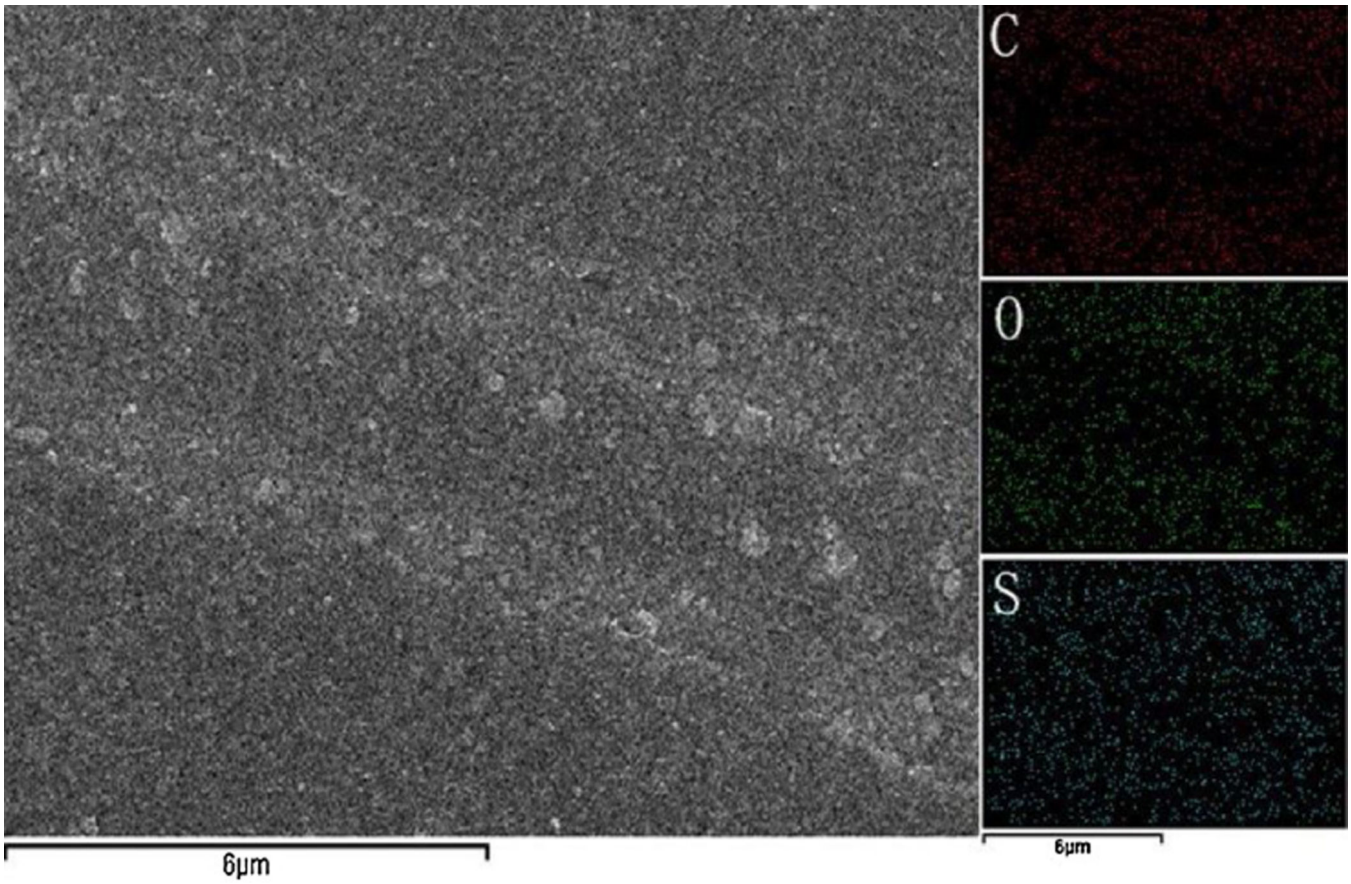

Fig. 3.
EDS mapping spectra of C, O and S in the grooved composite film.

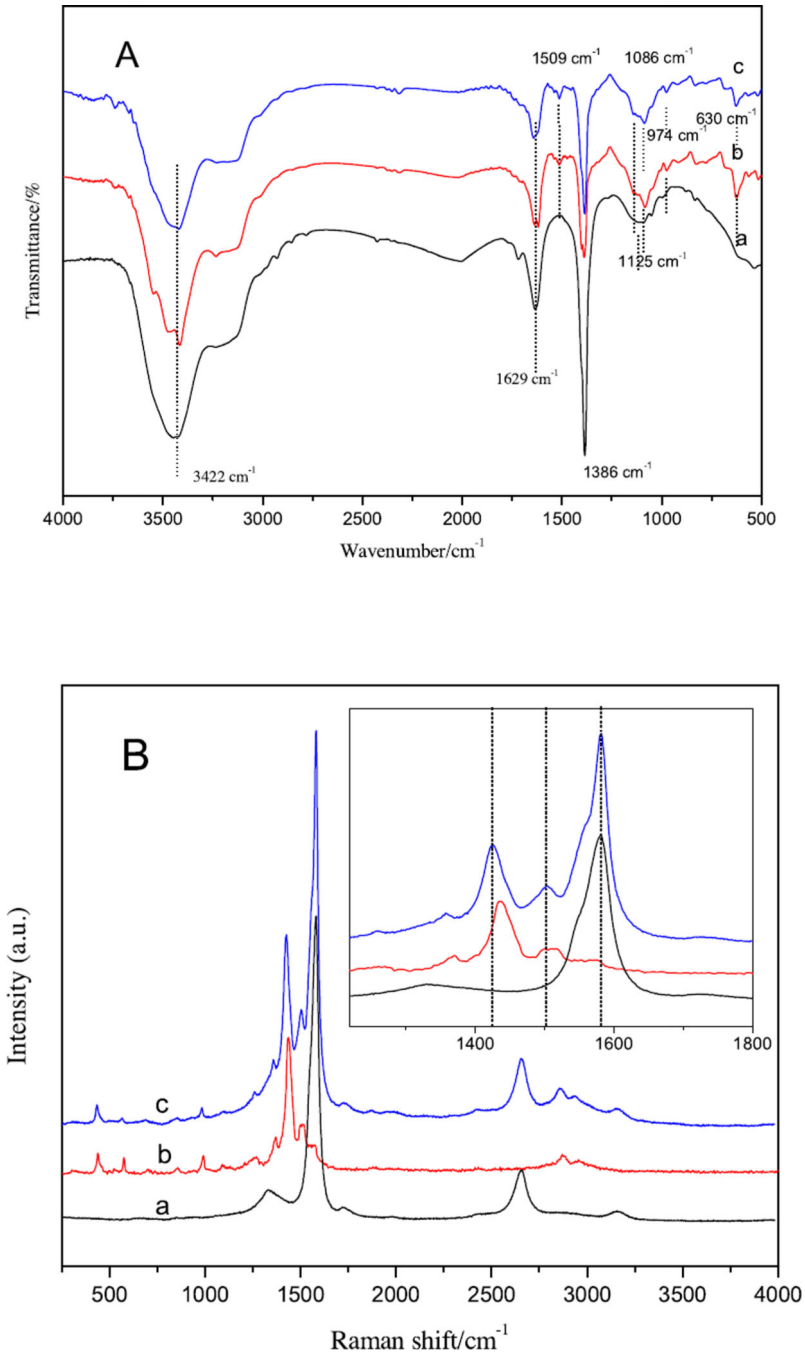

Fig. 4.

A. FTIR spectra of the SWNTs (a), PEDOT (b) and SWNT/PEDOT composite (c).(Spectra are shifted vertically for ease of view). B. Raman spectra of the SWNTs (a), PEDOT (b) and SWNT/PEDOT composite (c). Inset is a magnified plot to better show the peak shift.

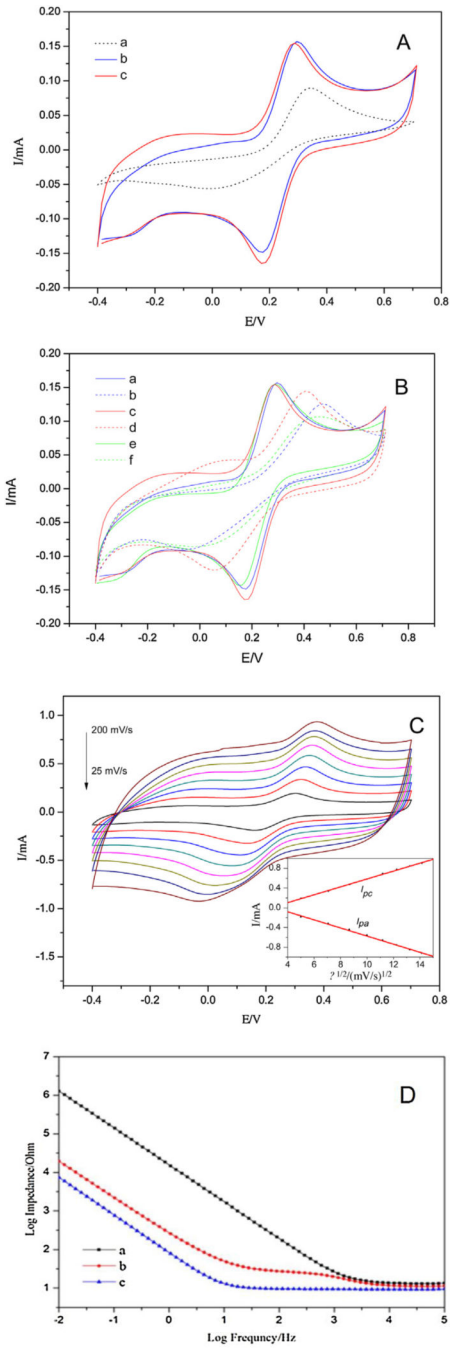

Fig. 5.

A. CVs of bare metal (a), grooved SWNT (b) and grooved SWNT/PEDOT (c) in 1 mM $[Fe(CN)_6]^{3-/4-}$ in 0.1 M KCl aqueous solution. Scan rate: 50 mV s^{-1}. B. CVs of the grooved SWNT (a: the 1 st cycle, b: the 200th cycle) and grooved SWNT/PEDOT(c: the 1 st cycle, d: the 200th cycle) modified electrode in 1 mM $[Fe(CN)_6]^{3-/4-}$ in 0.1 M KCl aqueous solution. Scan rate: 50 mV s^{-1}. CVs of the SWNT with PLA template are displayed as control (e: the 1 st cycle, f: the 200th cycle). C. CVs of the grooved SWNT/PEDOT with various scan rates from 25 to 200 mV s^{-1}. Inset shows the relationship between the peak current and the square

root of the scan rate. D. EIS of the bare electrode (a), grooved SWNT coated electrode (b) and grooved SWNT/PEDOT coated electrode (c).

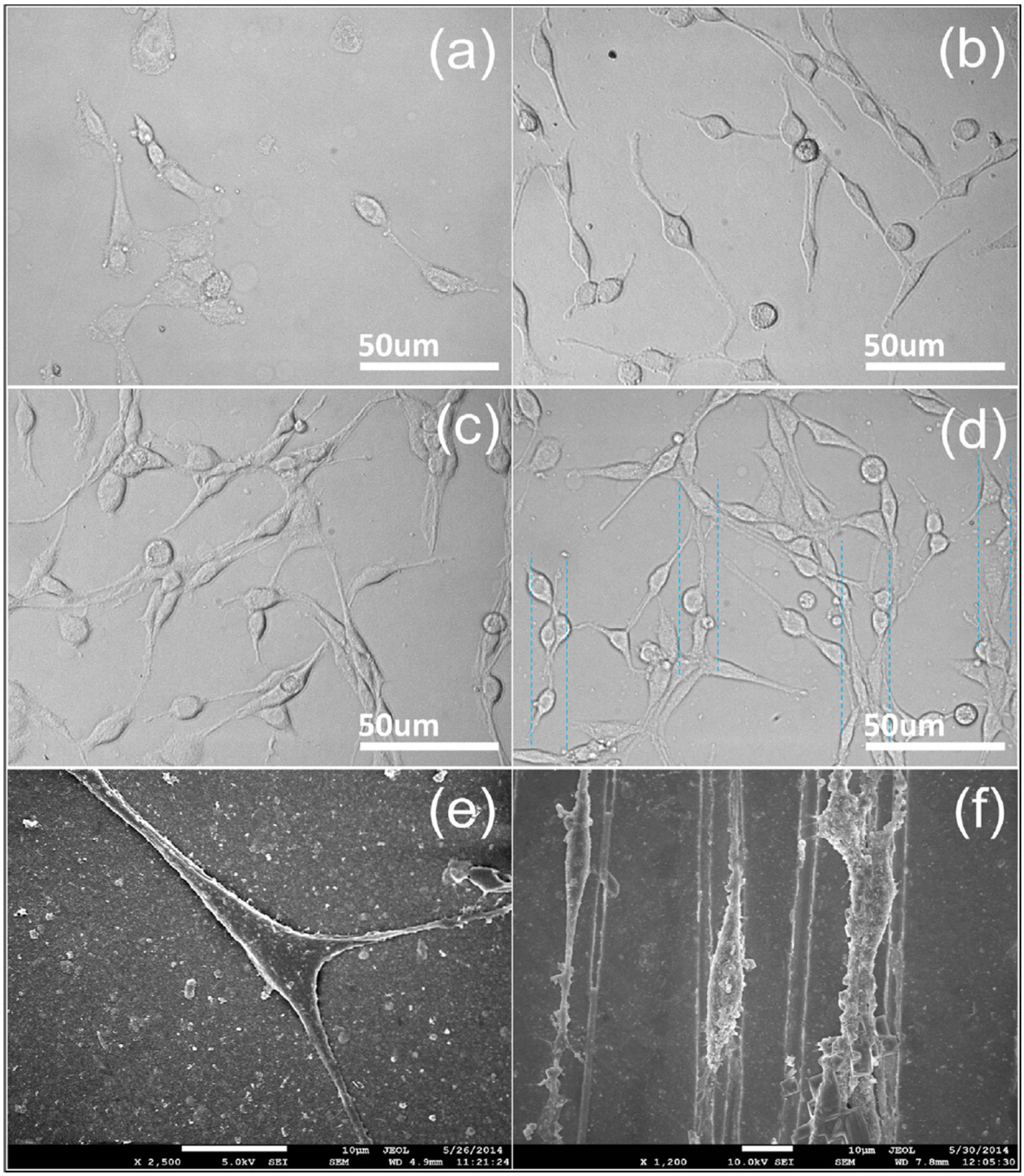

Fig. 6.

Micrographs showing PC12 cells cultured on different substrates at day 7: (a) bare electrode, (b) SWNT, (c) SWNT/PEDOT, (d) grooved SWNT/PEDOT. FESEM images showing PC12 cells grown on SWNT/PEDOT (e) and grooved SWNT/PEDOT (f).

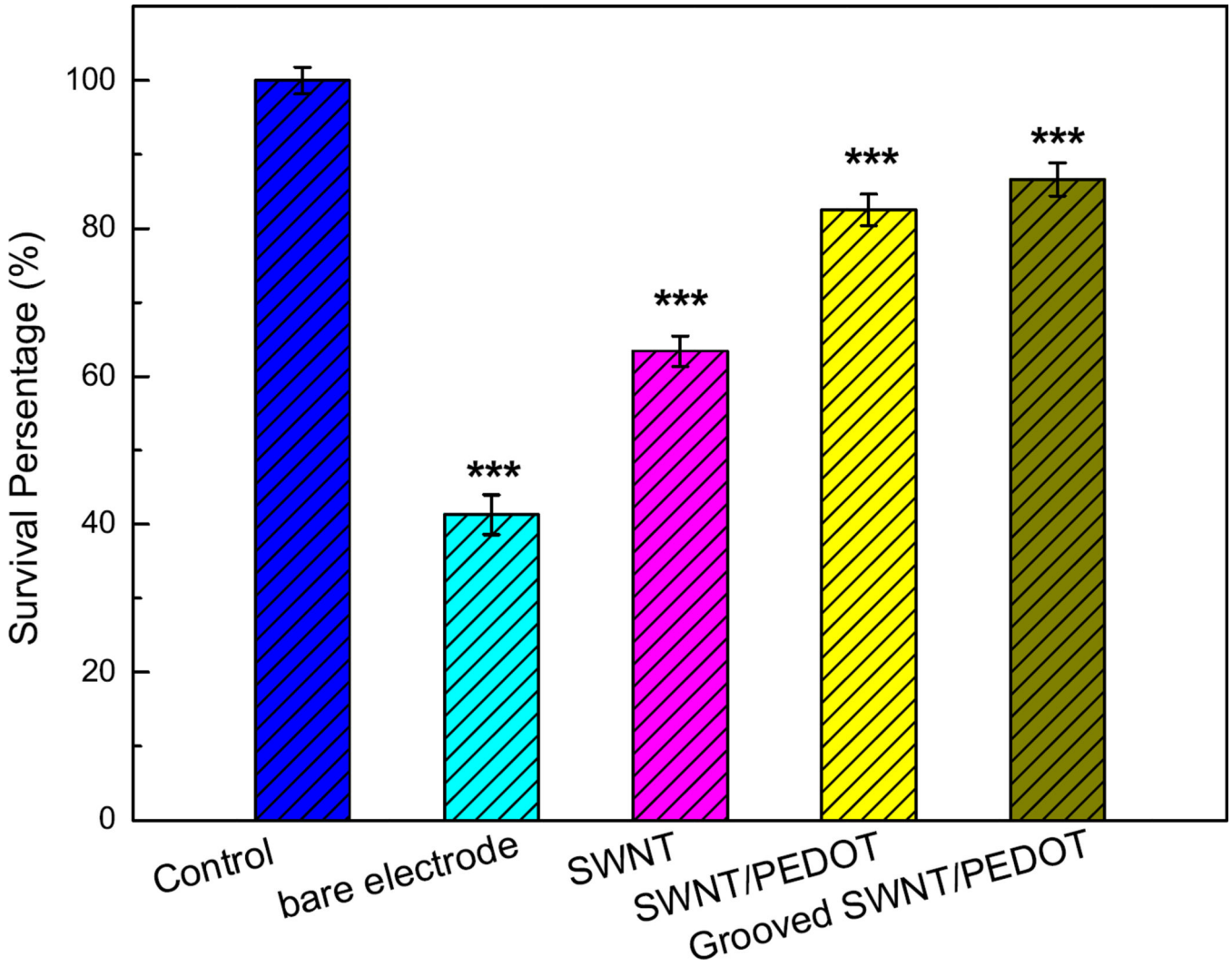

Fig. 7.

Viability of PC12 cells cultured on different surfaces. Data are shown in terms of mean ± SD (***$p < 0.01$ versus cells cultured in complete media).